AAS 24-151

PERTURBATION MODELING AND NAVIGATION TUNING FOR A CREWED STATION IN NEAR RECTILINEAR HALO ORBIT

Clark P. Newman[*], Jacob R. Hollister[†], and Diane C. Davis[‡]

NASA's Gateway program will build a crew-tended station in an Earth-Moon Near Rectilinear Halo Orbit (NRHO) to support deep space missions to the lunar surface and heliocentric space. The station in the NRHO will be visited by crewed vehicles including lunar landers that are high mass relative to Gateway. Docking events with large vehicles induce significant thruster plume and docking contact velocity perturbations. Crewed vehicles induce significant venting perturbations that can stress the navigation filter's ability to remain converged about an estimated state. The torques that arise from venting and lunar gravity gradient require reaction control system (RCS) thruster intervention, which themselves induce a velocity perturbation. The best method to model RCS thruster perturbations is currently in development. This paper simulates different RCS perturbation models, schedules, and an increasing magnitude to investigate the navigation sensitivity to different RCS perturbation models. From the RCS perturbation models simulated, a worst-case scenario is chosen for further scrutiny. The navigation filter is further tuned to handle the most disruptive perturbation modeling and the resulting performance is analyzed.

INTRODUCTION

Gateway Mission

NASA will place a crew tended station within an Earth-Moon southern L2 NRHO to support crewed missions in cislunar space and heliocentric space.[1] The specific orbit chosen has a lunar synodic resonance of 9:2, with a perilune radius near 3,400 km and an apolune radius near 70,000 km.[2] This orbit has a period of approximately 6.5 days and is characterized by long periods of low relative velocity punctuated by high velocity perilune passes. A primary mission of Gateway is to support the arrival of a crew via Orion and arrival of a Human Lander System (HLS), and to serve as the staging point for a lunar surface sortie with the HLS. A depiction of the HLS mission concept is shown in Fig. 1.

The NRHO phase of the Gateway mission begins with the Power and Propulsion Element (PPE) and Habitation and Logistics Outpost (HALO) maintaining the orbit shape and phase with orbit maintenance maneuvers (OMMs) nominally executed once per NRHO revolution.[3] While uncrewed, OMMs are executed with electric propulsion (EP), and while crewed they are executed with Reaction Control System (RCS) thrusters. During a lunar mission, HLS, Orion, and a logistics module (LM) arrive and perform the first lunar sortie through Gateway before departing.

[*]Project Engineer, a.i. solutions, Inc., clark.p.newman@nasa.gov
[†]Project Engineer, a.i. solutions, Inc., jacob.r.hollister@nasa.gov
[‡]Aerospace Engineer, NASA, diane.c.davis@nasa.gov

For this paper, two notional HLS mission timelines are considered, simulated, and evaluated. In both scenarios, the LM is first to arrive at the Gateway, and the crew and HLS arrive in two subsequent docking events, but the order of arrival differs. The first notional HLS mission considers HLS arriving and docking to Gateway before the crew, and the second mission assumes the crew arriving first. After successful docking, both missions assume HLS departs the Gateway for a one-revolution lunar surface sortie (labeled Depart to LLO in Fig. 1). After one revolution of the Gateway in NRHO, HLS returns and docks to Gateway after perilune passage (labeled Return from LLO in Fig. 1). With the lunar sortie complete, the crew relocate to the return vehicle and depart, HLS departs, and the logistics module departs, ending the lunar mission. Each docking and undocking event yields a distinct Gateway configuration; that is, a distinct combination of vehicles at specified docking ports.

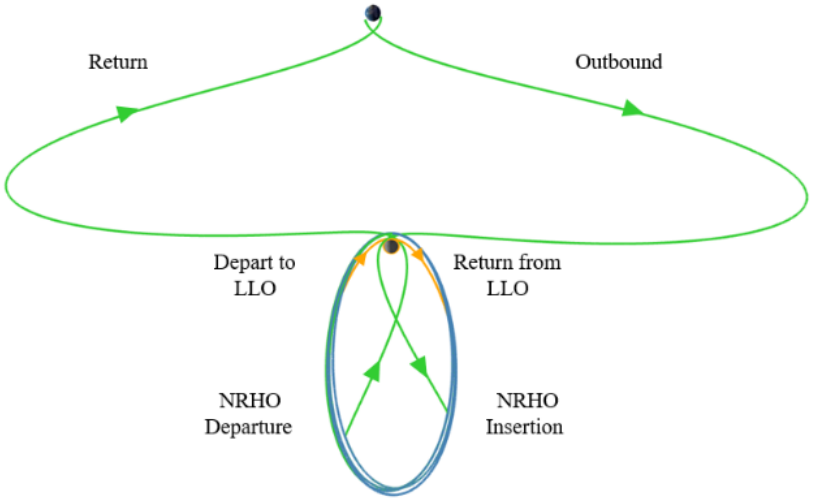

Figure 1: Lunar mission concept: the NRHO in blue, surface excursions in orange, and direct transfers in green, as viewed in the Earth-Moon rotating frame.

Gateway mission operations can be notionally split into two phases: a quiet uncrewed phase and a noisy crewed phase. To target OMMs and to plan rendezvous and proximity operations (RPOD) with visiting vehicles (VV), accurate knowledge of the Gateway state and predictions of the state to future events are important. While uncrewed, Gateway orbit is perturbed by solar radiation pressure (SRP), RCS desaturation maneuvers, and force mismodeling. While crewed, it is additionally perturbed by RPOD plume and contact forces, CO_2 venting, and additional RCS perturbations from near-continuous active control to maintain 3-axis attitude. The complications in navigation from these RCS perturbations are explored in this paper.

Tracking Data Schedule

For this analysis, the Gateway is tracked by the Deep Space Network (DSN), which provides coherent tracking data that includes X-band range and range-rate observations from its three primary sites at Goldstone (California), Canberra (Australia), and Madrid (Spain). The tracking schedule is variable depending on mission phase. During uncrewed periods, the Gateway is assumed to be tracked with three passes per NRHO revolution. In Figure 2, a diagram representing the NRHO shows three segments labeled A, B, and E. Orbit Maintenance Maneuvers (OMMs) are executed at true anomaly $\nu = 200^\circ$ and labeled OMM.[3] Each segment represents a 24 hour span within which

a contiguous 8-hour contact with a DSN site is selected to be the tracking data pass. Segment A contains the post-OMM tracking pass, segment B contains the post-perilune pass, and segment E contains the pre-OMM pass. The data cutoff (DCO) for final OMM targeting is at the end of segment E, which ends twenty-four hours before OMM execution.[4,5]

In addition to the nominal uncrewed tracking cadence, additional tracking data arcs are assumed to take place during RPOD event epochs. For this analysis, it is assumed that RPOD events are executed in the center of a sixteen hour tracking data span, with eight hours of tracking data on either side of the event epoch when possible. Note that there are cases of RPOD events occurring within eight hours of each other in both mission timelines. Finally, it is assumed for these analyses that the Gateway is tracked continuously when a crew is present.[6]

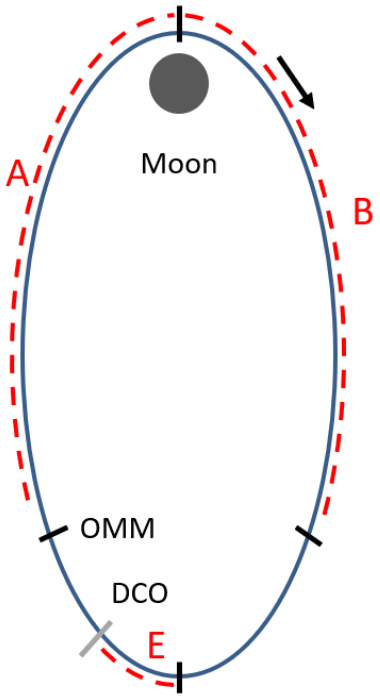

Figure 2: Nominal tracking data arcs visualized on the NRHO for uncrewed operations.

At times, the view of a tracking groundsite by the high gain antennas (HGAs) on board PPE is obstructed by Gateway or VV structure. The plane of the 9:2 lunar synodic southern L2 NRHO rotates in time with respect to the Sun, and the Gateway nominally maintains attitude in reference to the Sun, so groundsite view blockage changes between NRHO revolutions. RPOD events are planned in relation to NRHO true anomaly, so the HGA blockage for a specific mission timeline can be adjusted by shifting the starting revolution forward or backward incrementally in time.

Parallel to this navigation analysis is a visibility analysis that directly investigates possible ground site viewing times from the vehicle HGAs. The analysis considers the trajectory of the vehicle, the structure of the vehicle, the locations of the HGAs, and their gimbaling characteristics to build a contact report for the span of the HLS mission. The contact report is a timeline of possible communications links for the duration of the HLS mission. Tracking data can thus only be transmitted during these unobstructed view times.

PERTURBATIONS AND ERRORS

The Gateway is subject to many velocity perturbations that can stress the navigation filter's ability to respond to the perturbations and keep estimation errors bounded. An increase in velocity perturbations can also increase the cost of OMMs to maintain the NRHO phase that avoids eclipses.[7] OMMs are modeled ideally in the estimated spacecraft and with pointing and magnitude filters in the truth spacecraft (see Figure 3). RCS thrusters execute desaturation maneuvers that incur a velocity perturbation. Docking events incur velocity perturbations from thruster plume impingement forces and docking contact forces. While the crew is present, frequent CO_2 venting is expected which perturbs the Gateway.[8] Additionally, the gravity gradient torques induced by the Moon on the large HLS can require RCS thruster intervention to maintain three-axis attitude control.

It is assumed that while the RCS thruster torques are balanced, a residual velocity perturbation

arises from unequal thruster timing and performance or misalignments. This paper investigates different methods of modeling the RCS perturbations and their resulting effects on the performance of navigation. During Active RCS Mode, the RCS thrusters respond to high torques that exceed the control torque capability of the Reaction Wheel Assemblies (RWAs). Each RCS thruster perturbation executed in Active RCS Mode is modeled in one of two ways: either as a small velocity perturbation that is purely random in direction for each event, or as a perturbation in a configuration-dependent body-fixed direction. The body-fixed direction is determined randomly for each Gateway configuration and persists until the next docking or undocking event changes the configuration. The RCS perturbation schedule is driven with a configuration and altitude dependent time table that is common between RCS model types and HLS mission profile.

SIMULATION

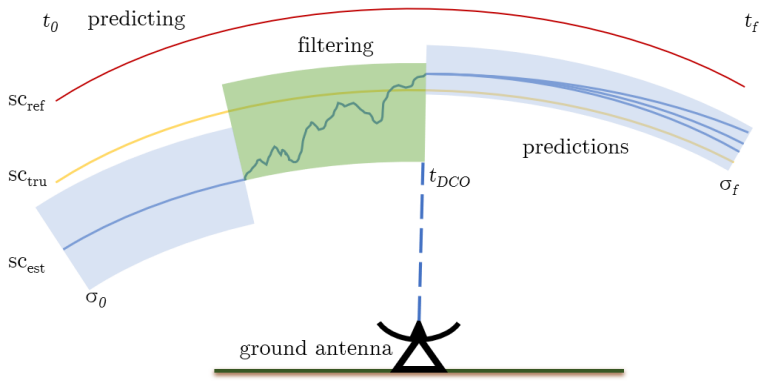

Figure 3: Diagram showing the estimated spacecraft sc_{tru} state updated by tracking data simulated on sc_{tru} in the Filtering phase, and multiple predictions originating from the final filtered state.

Simulation Overview

The navigation simulation works by modeling a truth and estimated spacecraft in the mission NRHO. Ground observations are simulated between the truth spacecraft and groundstation, which are then processed in a square root information filter (SRIF) to update the state of an estimated spacecraft. As depicted in Figure 3, the estimated spacecraft is associated with an uncertainty represented as the width of the blue area. When tracking data is processed, as in the green region, the estimated state of sc_{est} is updated and the uncertainty in that state is usually reduced.

The navigation simulation is run on the two notional mission timelines for a crewed arrival, lunar surface sortie, and departure. For each timeline, the perturbation modeling is first simplified to establish a baseline navigation performance in the absence of perturbations. Perturbation sources are activated in singular progression to isolate their impact on navigation performance. The navigation process is not re-tuned for each perturbation modeling scenario. For each mission timeline, the RCS perturbations are modeled as either a fully random or configuration-dependent body-fixed ΔV. A notional RCS perturbation schedule for each configuration is generated and the magnitude of the perturbations are increased until navigation performance deteriorates. Structural obstructions of ground site views are then considered, reducing tracking data availability during each mission timeline.

A Monte Carlo analysis is performed on both mission timelines, utilizing both methods of modeling RCS perturbations, and considering the structural obstruction timelines for each mission. First, the mission timelines are simulated with only the docking perturbations considered to establish a baseline performance. Next, venting perturbations are added to the truth spacecraft and the simulations are re-executed to isolate the effects of venting on navigation performance. RCS perturbations are then added, using both models per mission timeline, to again isolate the navigation performance changes due to the perturbation addition. Finally, the tracking data is restricted to only times where views to groundsites are unobstructed.

The schedule of RCS perturbations is common for both methods of RCS perturbations. However, the schedule is configuration and altitude dependent, becoming more frequent for larger configurations and at lower altitudes due to increased gravity gradient torques. For each RCS perturbation model, the perturbation magnitude is incrementally increased until the filter performance shows many diverging cases from the Monte Carlo analysis.

After the navigation performance sensitivities to different RCS perturbation models are established, more scrutiny is paid to the most stressing scenario. Additional tuning measures are employed in the stressing scenario to improve robustness against the perturbative flight regime. Rejected range intervention is applied to combat filter divergence due to filter collapse. Rotating velocity process noise components are applied to provide a finer tuning method in the context of navigation in the NRHO using Earth-based ground tracking.

Mission Timelines

RCS perturbations are explored for two notional HLS mission timelines, denoted mission timeline A and mission timeline B. The timelines of the two notional HLS mission appear in Table 1 and Table 2. Both simulated missions start on the first revolution and end after the ninth revolution. The NRHO revolution numbers in bold indicate revolutions in which a crew is present, placing the Gateway under near-continuous tracking. In mission timeline A, summarized in Table 1, HLS arrives on the second revolution, and the crew arrives after on the fourth revolution. In mission timeline B, summarized in Table 2, the crew arrives on the fourth revolution, and HLS arrives on the fifth revolution. Both notional timelines align with published HLS operations concept for Artemis IV.[9]

Table 1: Timeline of events for notional HLS mission A

NRHO revolution	Event
1	LM docks
2	HLS docks
4	Orion delivers module and relocates
4	LM relocates
5	HLS undocks for lunar sortie
6	HLS returns from lunar sortie
7	Orion undocks for Earth return
7	HLS undocks for departure
8	LM undocks for departure

Table 2: Timeline of events for notional HLS mission B

NRHO revolution	Event
4	Orion delivers module and relocates
4	LM docks
5	HLS docks
6	HLS undocks for lunar sortie
7	HLS returns from lunar sortie
8	Orion undocks for Earth return
8	HLS undocks for departure
9	LM undocks for departure

When HLS arrives for the first time to the Gateway in both missions it is in a heavy configuration loaded with propellant for the lunar surface sortie. On revolution 5 of HLS mission timeline A and revolution 6 of HLS mission timeline B the HLS departs for the lunar surface sortie and returns after one NRHO revolution. The Gateway actually traverses two perilune passages in this time, which is a region of increased dynamical sensitivities that magnifies errors. When the HLS returns after the lunar sortie it is in a light configuration having expended much of its lunar sortie propellant.

Every RPOD event perturbs the Gateway from vehicle thruster plume impingement on the Gateway structure and contact forces of the vehicle docking to Gateway. Not surprisingly, RPOD events associated with the heavy HLS result in the largest disturbances to Gateway. The RPOD perturbation is not known to the navigation filter, but the velocity uncertainty is increased per the magnitude of the RPOD event.

Perturbation Schedule

As mentioned previously, the HLS missions will be subject to RCS perturbations from maneuvers performed by the large integrated Gateway configurations that include Orion, HLS, or both. To explore the sensitivity of navigation performance to RCS perturbation modeling, two RCS perturbation models are considered (using a common perturbation schedule), and the magnitude of the modeled perturbations are incrementally increased until the navigation filter fails to stay converged through the entire mission timeline. It is assumed the RCS perturbations will be qualitatively characterized as small and frequent to emulate near-continuous attitude control from RCS thruster firings. It is also assumed that the impact of gravity gradient torques on the integrated Gateway configuration is stronger near perilune which will increase the rate of RCS maneuvering to maintain attitude control.

From these assumptions, an RCS perturbation schedule is prescribed for both mission timelines. In Tables 3 and 4, the time between RCS perturbations for each mission are detailed for altitudes above and below 10,000km. The number of fully-random desaturation maneuvers for uncrewed configurations are shown in the far right column. The simulation applies RCS perturbations during the mission per the rates described in Tables 3 and 4.

Table 3: RCS Perturbation schedule for notional HLS mission 1

NRHO rev	Event	Min per ΔV at radii (km) $>10^5$	Min per ΔV at radii (km) $<10^5$
1	LM docks	n/a	n/a
2	HLS docks	15	5
4	Orion delivers module and relocates	15	5
4	LM relocates	15	5
5	HLS undocks for lunar sortie	n/a	10
6	HLS returns from lunar sortie	15	5
7	Orion undocks for Earth return	15	5
7	HLS undocks for departure	n/a	n/a
8	LM undocks for departure	n/a	n/a

Table 4: RCS Perturbation schedule for notional HLS mission 2

NRHO rev	Event	Min per ΔV at radii (km) $>10^5$	Min per ΔV at radii (km) $<10^5$
4	Orion delivers module and relocates	n/a	10
4	LM docks	n/a	10
5	HLS docks	15	5
6	HLS undocks for lunar sortie	n/a	10
7	HLS returns from lunar sortie	15	5
8	Orion undocks for Earth return	15	5
8	HLS undocks for departure	n/a	n/a
9	LM undocks for departure	n/a	n/a

Other Error Sources

In addition to the RCS perturbations, other perturbations and errors are implemented in the simulation. In Table 5, the nominal error sources and their magnitudes are shown. The tracking data error statistics for DSN X-band data appear in Table 6.

Table 5: Simulated Error Sources

Parameter Name	1-σ uncertainty
Initial Position Error	10 km
Initial Velocity Error	1 cm/s
Relative Mass Error	30%
Relative SRP Area Error	30%
Desaturation Maneuver ΔV	3.33 mm/s 1
Uncrewed OMM Constant Error	0.47 mm/s
Uncrewed OMM Magnitude Error	0.5%
Crewed OMM Magnitude Error	0.5%
OMM Pointing Error	0.333°

[1] Desaturation occurs once before OMM execution and three times at perilune for both uncrewed and crewed configurations.

Table 6: Tracking Data Quality Parameters

Parameter	Value (1-σ)
Range Noise (m)	1.0
Range Bias (m)	7.5
Range-Rate Noise (mm/s)	0.1

Finally, varying perturbations from CO_2 venting and wastewater dumping by crewed configurations are considered. The venting schedule is input to the navigation simulation from simulations performed for attitude control analyses via log files.

To summarize: this analysis simulates a Gateway that supports an HLS mission where the crew and lander pass through the Gateway to the lunar surface and back. Two timelines of an HLS mission are considered and simulated in a navigation and astrodynamic simulation. Tracking data is generated for a truth spacecraft over both mission timelines, and a navigation filter estimates its state through the estimated spacecraft state. Several errors and perturbations are implemented in the simulation that are described above. Of primary interest in this analysis are the many small perturbations that come from active RCS control to maintain three-axis attitude control.

NOTIONAL HLS MISSION TIMELINE A

Error Sensitivities

The first analysis on HLS mission timeline A activates new error sources singularly to isolate navigation performance changes due to force modeling updates. To establish a baseline performance of the navigation filter on HLS mission timeline A, a monte carlo simulation is run on that mission timeline without consideration to visiting vehicle venting, RCS perturbations, or antenna blockages. In Figure 4a the position and velocity 3-σ uncertainties of each monte carlo iteration are plotted over the timespan of HLS mission timeline A.

Perilune passes are distinct as the peaks of position and velocity uncertainties in Figure 4a. Tracking passes are highlighted as pink and light blue for position and velocity, respectively, and contribute to reducing the uncertainties. The arrival of Orion begins constant tracking, noted as the extended period of highlighted curves. The sawtooth pattern results from hemispherical handovers involving Canberra station, where the tracking groundsite switches from northern to southern hemisphere or vice versa.[10] The velocity uncertainty is inflated at RPOD epochs (marked as vertical

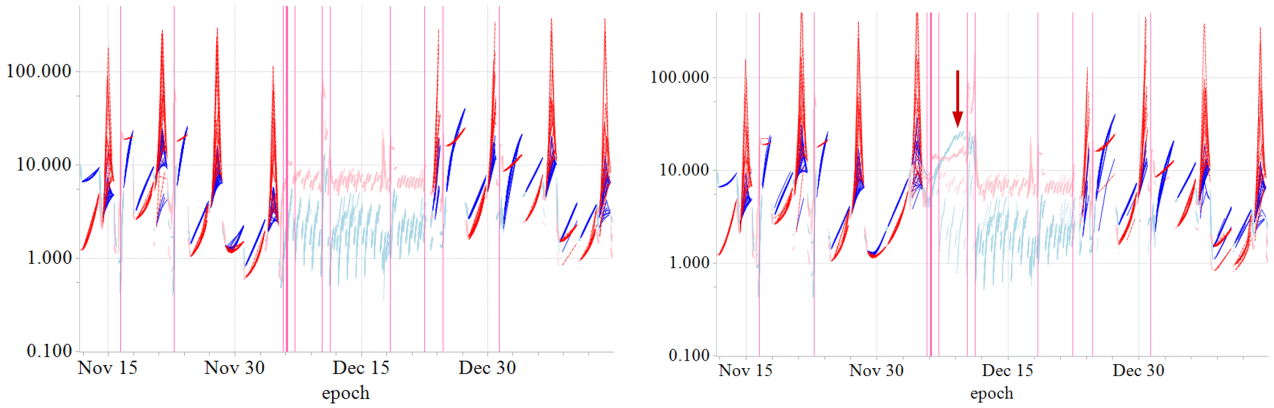

(a) Baseline

(b) With venting

Figure 4: 3-σ uncertainties for position (blue) and velocity (red) over the course of HLS mission timeline A. Lighter colors indicate periods of active tracking. Vertical bars are RPOD epochs.

bars) commensurate with the RPOD perturbation magnitude. The most notable event is the HLS undocking for the lunar sortie on revolution 5, where the velocity uncertainty is much higher on the right side of the event. This RPOD event is marked in Figure 4a by a bold vertical bar. The HLS return after 18 December shows a smaller increase in velocity uncertainty which quickly returns to the steady-state range of values. Around 24 December Orion departs, ending the constant tracking. After Orion's departure, HLS and LM each depart the Gateway, and two revolutions of uncrewed flight follow as the navigation performance returns to its steady state.

Next, the vent model in the navigation simulation is activated to isolate the changes in navigation performance due to the increased disturbances. The resulting navigation filter state uncertainties are shown in Figure 4b. The most notable difference from the addition of venting is the increase in uncertainties in the early span of the crewed portion of the mission, particularly of position uncertainty. The navigation filter is tuned for the baseline force model scenario shown in Figure 4a and is not adjusted thereafter for each force model scenario. The error sources are added sequentially, and then the RCS perturbation magnitude is increased incrementally.

In the next phase of the analysis, RCS perturbations associated with attitude control are included. In Figure 5a, each perturbation is applied in a random direction, while in Figure 5b, a body-fixed direction is randomly selected with each Gateway configuration change (i.e., at each RPOD event) and applied for the duration of that configuration. The RCS perturbations follow the schedule in Table 3. The fully random scenario executes RCS perturbations of 1 mm/s while the body-fixed RCS perturbations have a magnitude of 0.1 mm/s.

In both scenarios shown in Figures 5a and 5b there are several cases where the position and velocity uncertainties rise unbounded for some or all of the timeline. One example is highlighted with a red arrow in Figure 5a. This growth is indicative of the navigation filter rejecting most observations and is considered diverged. For cases that do not diverge, the performance is comparable to the scenario that considers CO_2 venting displayed in Figure 4b.

Finally, the tracking data is restricted to times in which there is not a structural blockage arising from the Gateway or VV structure. The HLS mission timeline A is simulated with a Gateway 3D model in the operational attitude and vectors to groudnsites to determine periods of structural

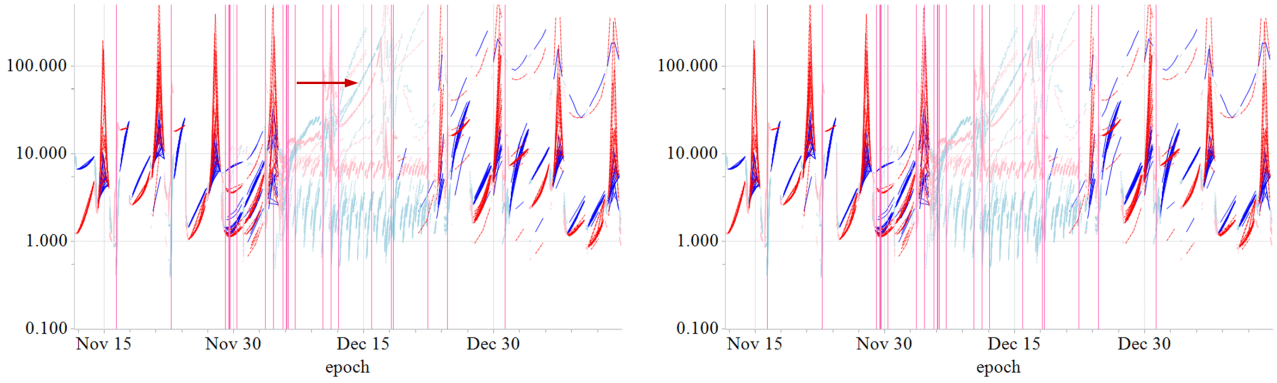

(a) Random (b) Body-fixed

Figure 5: 3-σ uncertainties for position (blue) and velocity (red) over the course of HLS mission timeline A with RCS perturbations activated. Lighter colors indicate periods of active tracking. Vertical bars are RPOD epochs.

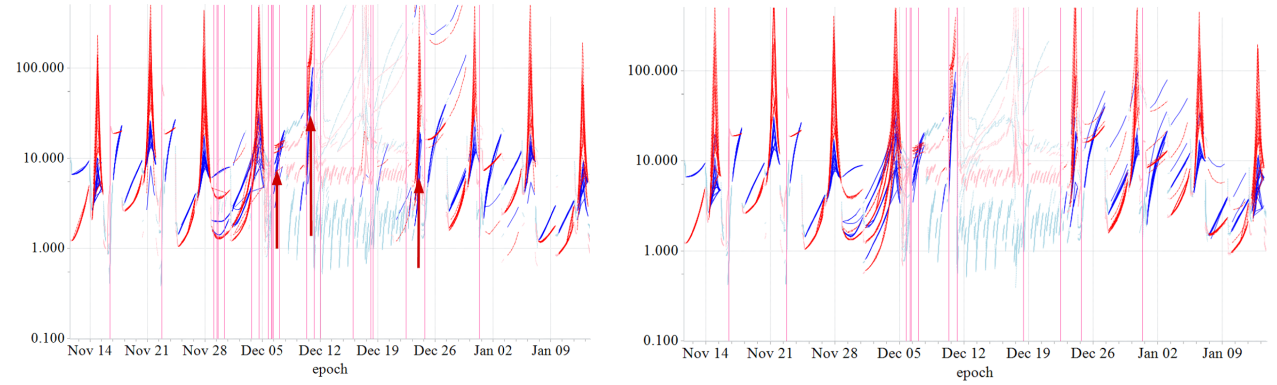

(a) Random (b) Body-fixed

Figure 6: 3-σ uncertainties for position (blue) and velocity (red) over the course of HLS mission timeline A with RCS perturbations activated and structural blockage considered. Lighter colors indicate periods of active tracking. Vertical bars are RPOD epochs.

blockage, and that data is utilized by the navigation simulation to restrict tracking data generation. In Figure 6, the 3-σ filter uncertainty for Gateway position and velocity over the HLS mission timeline A are shown for the scenario that considers structural blockage and RCS perturbations. The scenario with 1 mm/s random perturbations is displayed in Figure 6a and the scenario with 0.1 mm/s body-fixed RCS perturbations is displayed in Figure 6b. Note that these two values are selected based on filter performance and represent the disturbance magnitudes at which the filter begins to diverge in each scenario. The fully random perturbations have a much smaller impact on the performance of the filter as compared to body-fixed perturbations.

There are some untimely structural blockage time spans that impact mission performance. These drops are marked with arrows in Figure 6a. There are two notable data drops early in the crewed phase right before important RPOD events, including the HLS departure for the lunar sortie. Both the random and body-fixed scenarios exhibit iterations that diverge unbounded. Overall, the questionable performance with RCS perturbations appears only slightly qualitatively worse with struc-

tural blockage when observing the filter 3-σ uncertainties over time.

To quantify the compounding effect of adding error sources, navigation state errors are compared at events of interest during the mission timeline. The impact of additional error sources is most evident at the HLS undock event on revolution 4 for the lunar sortie. In Figures 7a and 7b, the position and velocity navigation error statistics immediately before the HLS undock event epoch on revolution 4 appear in a box-wing plot for each error model scenario.

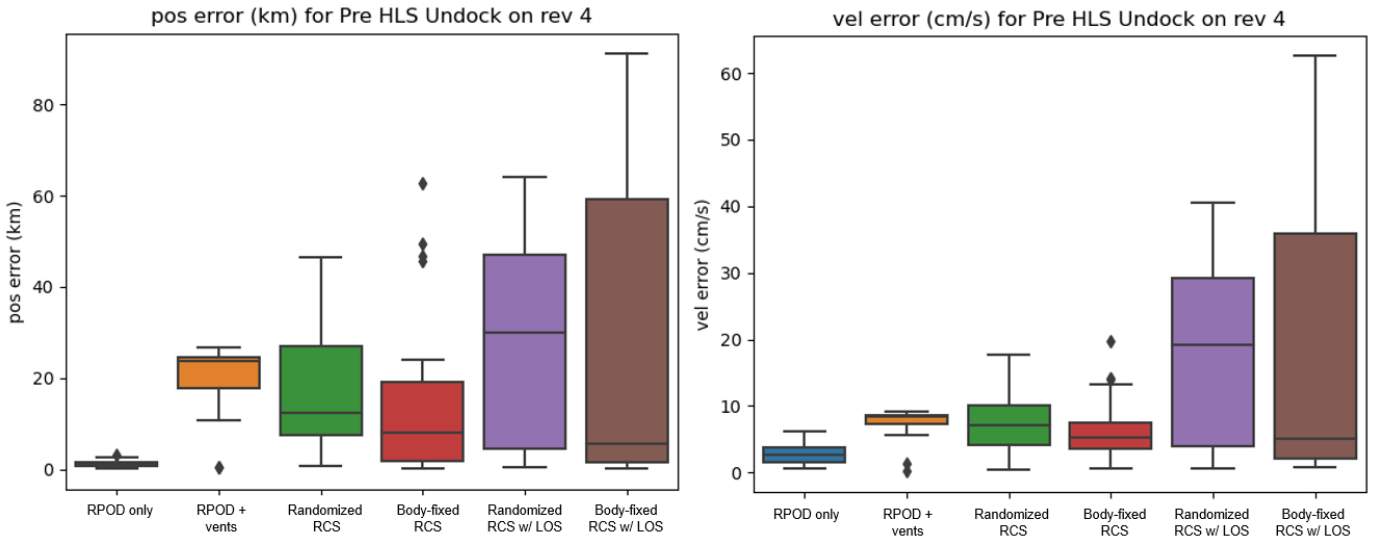

(a) Position

(b) Velocity

Figure 7: Error statistics prior to the HLS undock event epoch on revolution 4 in HLS mission timeline A for scenarios of increasing number of error sources.

The inclusion of antenna blockage for the mission has the largest impact on errors at this event in this timeline. The specific timing of antenna blockages to Earth is time-dependent so shifting the starting revolution of this mission will in turn move or remove blockages from before critical events in the mission timeline. Once HLS has departed for the lunar sortie, the perturbations and antenna blockages in this timeline subside, so that the navigation filter performance is insensitive to their inclusion in the simulation. This insensitivity is evident in Figures 8a and 8b, which show the position and velocity error statistics immediately prior to HLS docking event epoch post-lunar sortie. The errors do not substantially grow from the inclusion of additional error sources.

RCS Perturbations

The analysis and figures shown in Figures 5a through 6b for the fully random and body fixed RCS perturbations have a prescribed magnitude of 1 mm/s and 0.1 mm/s, respectively. To further understand the impact of RCS perturbation model and magnitude to navigation performance in this mission timeline, monte carlo simulations are performed for each RCS perturbation model and the magnitudes of the perturbations are increased as the performance of the navigation filter is documented. The filter is not re-tuned for each scenario, so the results are direct comparisons to isolate the navigation performance change due to the perturbation magnitude.

In Figures 9a and 9b, the data performance statistics are displayed for HLS mission scenarios of increasing perturbation magnitude in box-wing plots showing the range observation acceptance

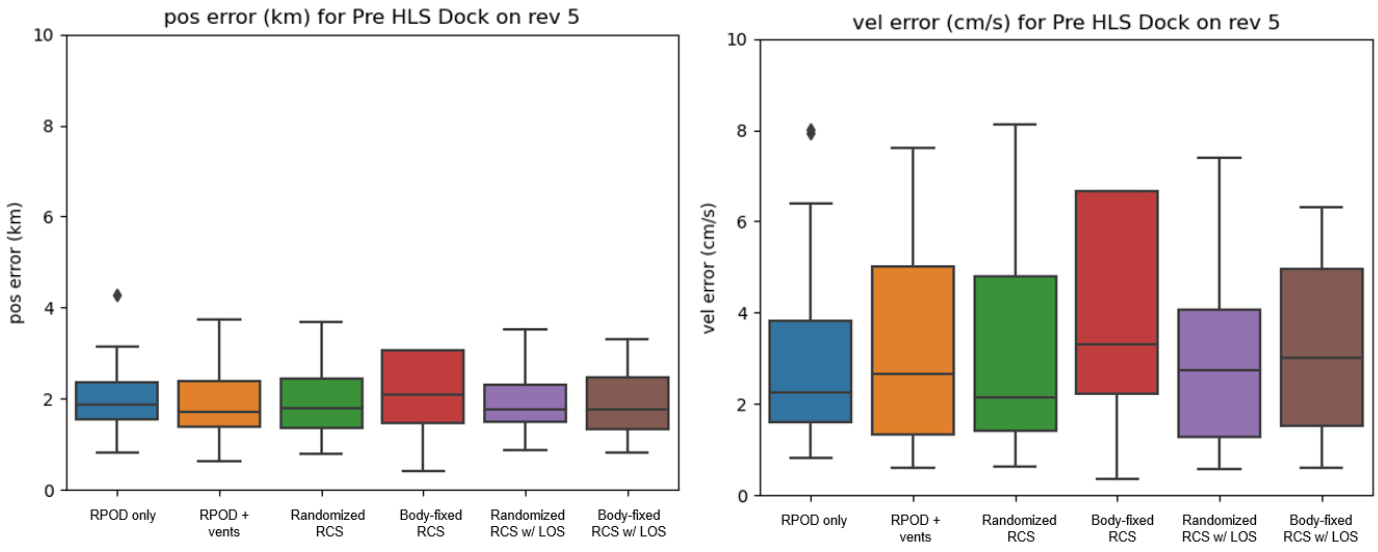

(a) Position

(b) Velocity

Figure 8: Error statistics at the HLS dock event epoch on revolution 5 in HLS mission timeline A for scenarios of increasing number of error sources.

rate. Observations whose pre-fit residuals are above the three sigma uncertainty are rejected and not included in a filter state update. For both RCS perturbation models applied to the HLS mission simulation, the range acceptance rate decreases with increasing RCS perturbation magnitude. The navigation filter is more sensitive to body-fixed RCS perturbations, with the range data acceptance rate falling quickly between 0.1 and 0.2 mm/s. This performance breakdown does not occur for the fully random RCS perturbation model of magnitudes below 1.0 mm/s.

To summarize, a fully random or body-fixed schedule of RCS perturbations as defined in Table 3 are applied to HLS mission timeline A (defined in Table 1). For each RCS perturbation model (fully random or body-fixed), a monte carlo analysis is run for cases of increasing perturbation magnitude. It is found that for this HLS mission timeline and during the epochs considered, the navigation performance degrades for RCS perturbation magnitudes above 2.0 mm/s and 0.2 mm/s for fully random and body fixed RCS perturbation models, respectively.

NOTIONAL HLS MISSION TIMELINE B

The same set of analyses is conducted on HLS mission timeline B, whose timeline is defined in Table 2. The most salient difference between mission timelines A and B is the order in which the HLS arrives- either before or after Orion's arrival. In notional HLS mission timeline B, HLS arrives after Orion's arrival. For this mission timeline the same steps are taken: the force modeling and data blockage are activated progressively to isolate the performance changes, and then the notional RCS perturbation models are applied with increasing magnitude.

Error Sensitivities

As with the first notional HLS mission timeline, a simplified simulation that does not consider venting, antenna blockage, or RCS perturbations is executed to document a baseline performance. Error sources are then added individually to isolate their impact to navigation performance. For this

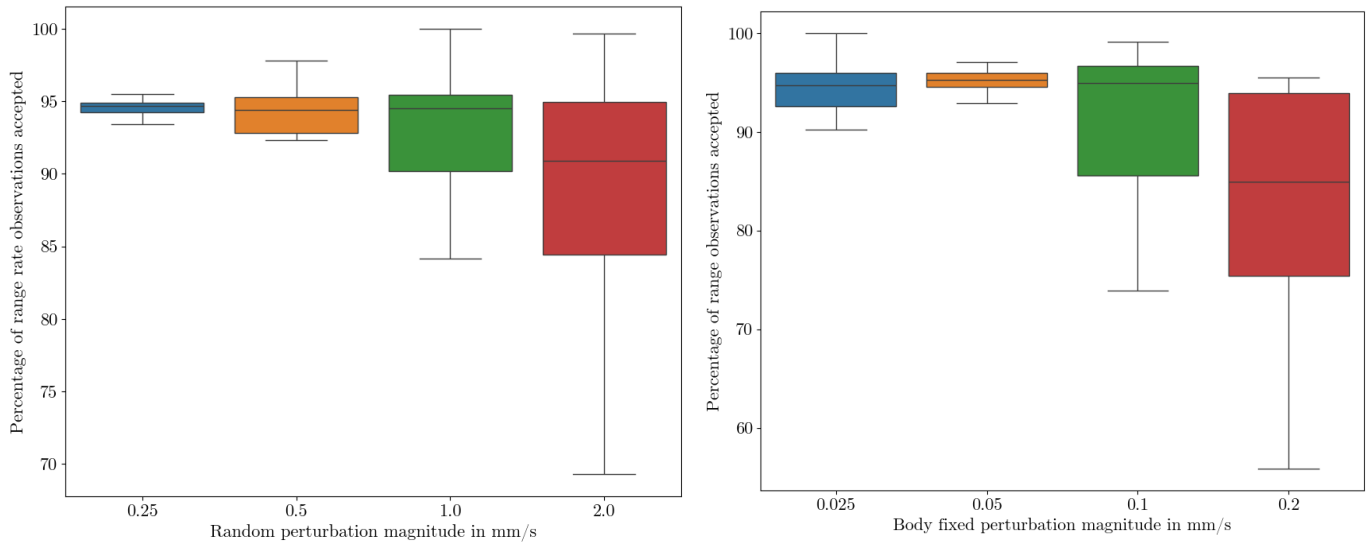

(a) Random

(b) Body-fixed

Figure 9: Percentage of range observations accepted for scenarios of increasing RCS perturbation magnitude on HLS mission timeline A.

mission timeline we will omit the buildup of error source scenarios and focus on the final scenarios that considers RCS perturbations and structural blockage.

Both RCS perturbation models are applied to HLS mission timeline B, as well as structural antenna blockage. The position and velocity 3-σ uncertainties over time are shown in Figures 10a and 10b for the fully random or body fixed RCS perturbation models, respectively. The fully random RCS perturbation model magnitude is set to 1.0 mm/s while the body fixed magnitude is 0.1 mm/s. Neither case includes monte carlo iterations that show signs of divergence. There are some notable data drop outs in the 1e timeline and this starting epoch, highlighted with arrows in Figure 10a. There is a data drop out between the first two RPOD events, as well as before the third RPOD event. After the HLS returns to Gateway post-lunar sortie on December 25 , there are two more data drop outs, including one that spans a perilune passage. Regardless, both scenarios perform under these conditions without divergence, and most of the mission uncertainties remain below 10 km and 10 cm/s when not in the vicinity of an RPOD event, data drop out, or perilune passage.

To assess accuracy at a critical RPOD event, the estimation error statistics at the HLS departure event on the fifth revolution for the progressive error models are shown in Figures 11a and 11b for position in km and velocity in cm/s, respectively. At this RPOD event, the navigation filter is robust against and insensitive to the addition of the listed error sources. The average error is below 2 km and 3 cm/s for both RCS perturbation models. The RCS perturbation magnitudes applied in this analysis are 1.0 mm/s and 0.1 mm/s for the random and body fixed models, respectively.

The HLS return event on the sixth revolution in Figures 12a and 12b displays similar behavior. The average error at this RPOD event for both RCS perturbation models are just above 1.0 km in position and 1.0 cm/s in velocity. The navigation performance is insensitive to the addition of the listed error sources.

To understand the sensitivity of the navigation performance to increasing RCS perturbation mag-

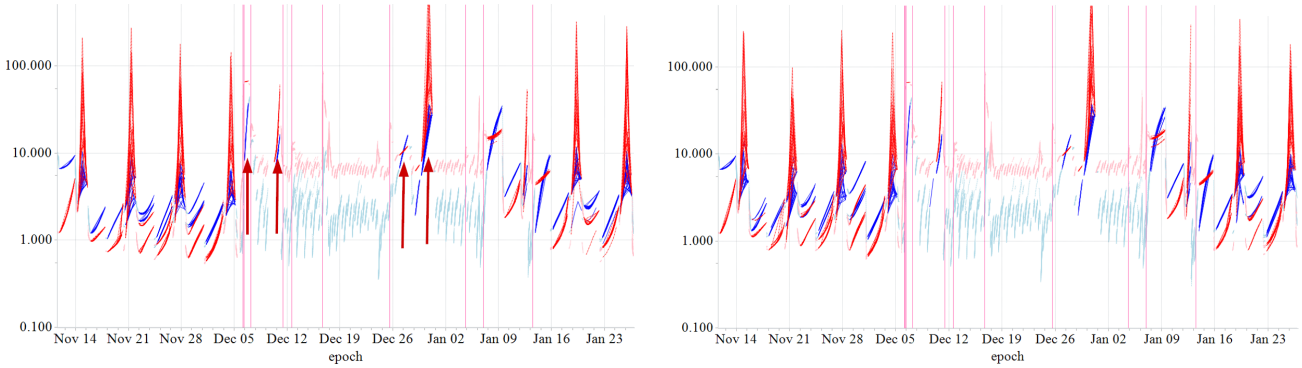

(a) Random

(b) Body-fixed

Figure 10: 3-σ uncertainties for position (blue) and velocity (red) over the course of HLS mission timeline B with RCS perturbations activated and structural blockage considered. Lighter colors indicate periods of active tracking. Vertical bars are RPOD epochs.

nitudes, and to assess the maximum magnitude the filter can handle, the perturbation magnitude for both models are increasedincreased, and their performance is documented. In Figures 13a and 13b the statistics of range observation acceptance for increasing RCS perturbation magnitudes are shown for the random and body-fixed RCS models, respectively. For HLS mission timeline B, the navigation filter performance degrades at higher magnitudes than in HLS mission timeline A. Navigation performance degradation begins between 5 and 10 mm/s for the fully random RCS perturbation model, and at 2 mm/s for the body fixed model. These are roughly an order of magnitude greater than the perturbations that the navigation filter could handle for HLS mission timeline A. These results are dependent on the starting epoch of the mission timeline and the tracking data assumptions held for the simulations.

The primary reasons for the difference in filter performance between the two timelines are associated with availability of tracking data. In mission timeline A, HLS arrives before Orion, so the uncrewed tracking cadence (3 tracks per revolution) is applied while HLS is docked prior to Orion arrival. Additionally, Sun-Earth-Moon geometry results in loss of tracking due to structural blockage during critical events in timeline A. In timeline B, Orion is present when HLS docks, so crewed tracking assumptions (constant tracking) are in place for the duration of the HLS stay at Gateway. Additionally, certain critical RPOD events occur one revolution later in time, such that the resulting shift in Sun-Earth-Moon geometry allows contact and tracking during those critical events. These results suggest two potential mitigation strategies. Filter behavior can be improved by commencing continuous tracking with the arrival of HLS if it docks prior to Orion. Additionally, applying spacecraft attitude strategies or careful mission epoch selection to increase tracking availability during critical events may significantly improve filter performance.

TUNING MEASURES

The analyses to this point do not re-tune the navigation filter for each force model scenario. Rather, the navigation filter is tuned for the baseline case that only considers RPOD perturbations, and then the perturbations and blockages are added progressively to isolate the performance changes to the different scenario models. Now some effort is taken to re-tune the navigation filter for some of the more stressing scenarios to recover a more contextual performance expectation.

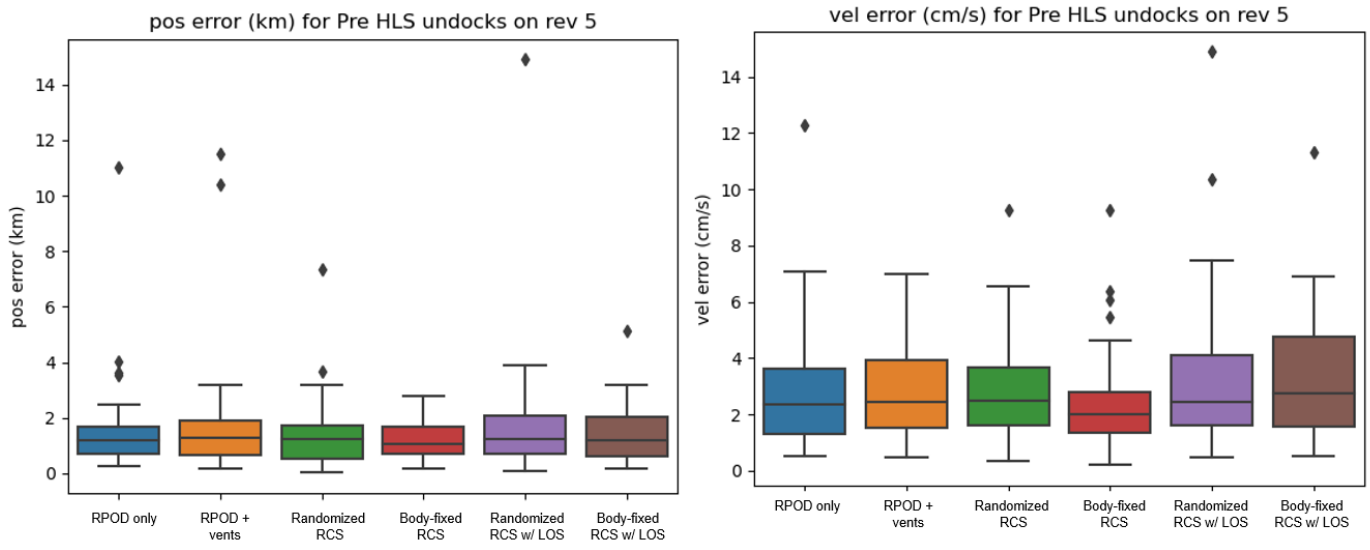

(a) Position

(b) Velocity

Figure 11: Error statistics at the HLS undock event epoch on revolution 5 in HLS mission timeline B for scenarios of increasing number of error sources.

Typically the first parameters to adjust to tune a navigation filter for a specific scenario or application are the process noise spectral density values. Increasing velocity process noise can aid the filter where there is solution ambiguity or force mismodeling. In the case of navigation in the NRHO, filter tuning is driven more by solution ambiguity. For much of the NRHO, there is be a wide set of solutions that can produce reasonable observation residuals. If the navigation filter is "collapsed" around an erroneous solution as evidenced by small covariance diagonal values, it has difficulty recovering to the "correct" solution. This is discussed further below.

In addition to the first step of increasing the magnitude of the velocity process noise, there are two more intricate methods of tuning explored to improve the navigation performance for the notional HLS missions with notional RCS perturbation models. The first is Range Rejection Intervention, where the filter slightly increases the position covariance along its shortest principal axis for each progressive range observation rejection due to sigma-editing. The second method is adjusting the input velocity process noise values so that they are defined in a rotating frame to allow contextual break down of the velocity process noise into discrete elements. This directional approach is a more intricate application of process noise over a spherical application of a single magnitude in each inertial direction.

Range Rejection Intervention

The course of these analyses reveals the propensity of the navigation filter to enter a "range-rate only" mode where range observations are sigma edited while range-rate observations are accepted. This selective rejection can cause the total filter error to grow unbounded while filter covariance remains bounded until the filter completely diverges and no observations are accepted. Ironically, it is when all observations are being sigma edited that the covariance also grows unbounded; with the covariance growth, it is possible for the filter to begin accepting observations once more.

The range-rate intervention method uses principal component analysis of the position covariance

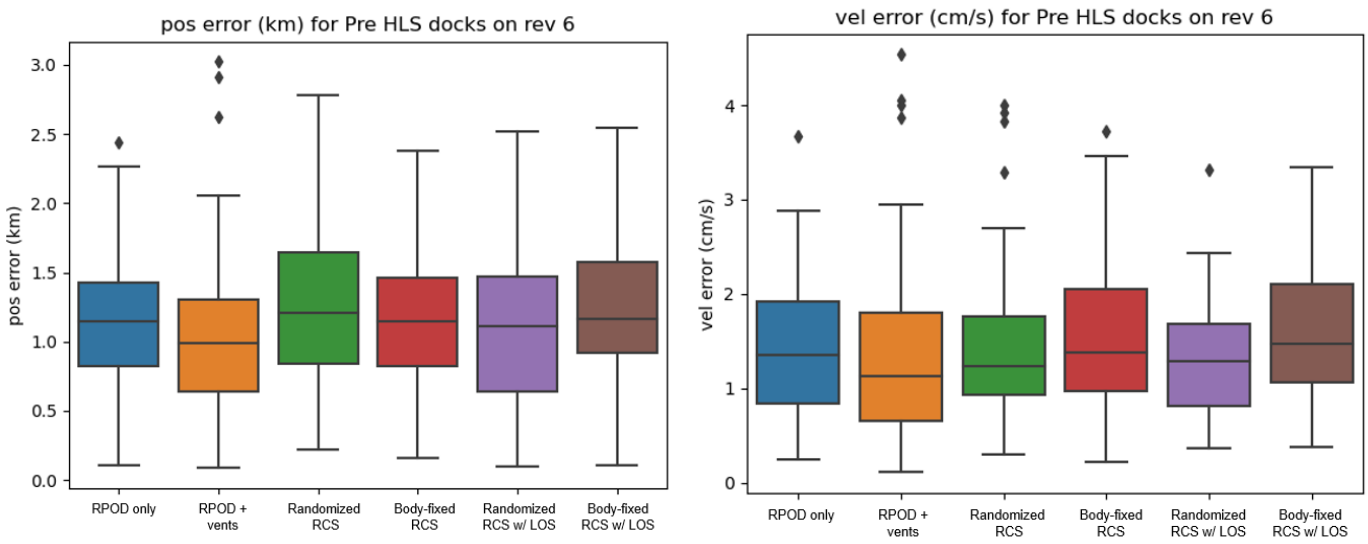

(a) Position

(b) Velocity

Figure 12: Error statistics at the post-lunar sortie HLS dock event epoch on revolution 6 in HLS mission timeline B for scenarios of increasing number of error sources.

by eigen decomposition. The eigenvector corresponding to the smallest eigenvalue represents the minor axis of the position covariance ellipsoid. In the NRHO regime, the smallest principal axis of the position covariance is typically aligned with the range observation direction.

Range observation sigma editing is dependent on the observation residual divided by the combined uncertainty in the range direction plus range observation noise. With the collapsed position covariance in the range direction, range observations can become sigma edited with much lower residual magnitude than if the covariance was rotated so the median or major axis are along the range observation direction.

Range rejection intervention is triggered if a range observation is sigma edited. The position covariance is then decomposed and the smallest eigenvalue identified. That eigenvalue is then multiplied by a coefficient slightly greater than one (1.1 in the simulation for this analysis), and the position covariance is recomposed.

Range rejection intervention could improve the robustness of the navigation filter against falling into "range-rate only" mode, allow it to accept more range observations overall, and improve performance. To test this, the scenario of HLS mission timeline A with body fixed RCS perturbations of 0.1 mm/s is revisited. The range acceptance statistics from the original simulation appear in Figure 9b. This scenario was re-executed with range-rejection intervention activated with the coefficient of 1.1. The range acceptance statistics and position error at HLS undock appear in Figures 14 and 15, respectively, for the nominal and range rejection intervention scenarios. Figure 14 shows that the range rejection intervention scenario has a lower whisker above 95% while the nominal scenario has a lower whisker below 75%. Additionally, Figure 15 shows that the inclusion of range rejection intervention improves position error statistics at the HLS undock for lunar sortie event on revolution 4. While the average error improves only slightly from 2 km to 1 km, the outliers reduce dramatically with the nominal top whisker at above 60 km, and the range rejection intervention top whisker below 10 km. For this scenario, range rejection intervention improves navigation robustness and

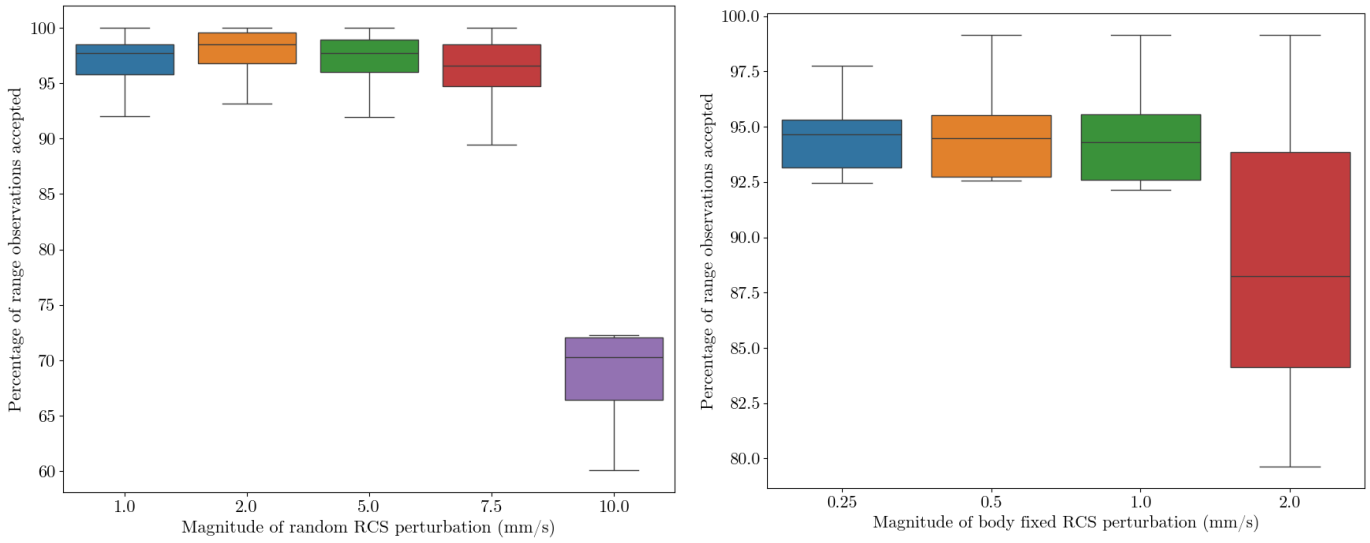

(a) Random

(b) Body-fixed

Figure 13: Percentage of range observations accepted for scenarios of increasing RCS perturbation magnitude in HLS mission timeline B.

performance.

Rotating Process Noise

The application of process noise empowers a navigation system to be robust against unmodeled or mismodeled error sources. The mathematically applied force model within the navigation filter is necessarily incomplete and contain errors and assumptions. Process noise is specifically a spectral density matrix added to the propagation equation for the navigation filter algorithm, and it is shown below in Equation 1.

$$\dot{\mathbf{P}}(t) = \mathbf{F}(t)\mathbf{P}(t) + \mathbf{P}(t)\mathbf{F}(t)^T + \mathbf{Q}(t) \tag{1}$$

Equation 1 describes how the covariance $\mathbf{P}(t)$ is propagated between observation updates. $\mathbf{F}(t)$ is the simulation force model, and $\mathbf{Q}(t)$ is the spectral density matrix that contains process noise values for each navigation filter state in its diagonal. For a state vector with six elements to define position and velocity, the velocity process noise is represented by the last three elements of the matrix diagonal.

The behavior of the process noise itself is a design point for navigation filter development. At its most basic, a single value for all simulation time occupies the last three diagonal elements. The navigation simulation developed for these analyses employs a spherical application of velocity process noise whose single-valued magnitude is configuration specific and can change with each RPOD event. E.g. a large and perturbative configuration likely necessitates a larger process noise magnitude than a smaller, more quiescent configuration.

The application of velocity process noise can also be non-spherical and rotate over time. This more complex application of process noise requires more information to be passed through the formulation of process noise values. For these analyses, a non-spherical velocity process noise is

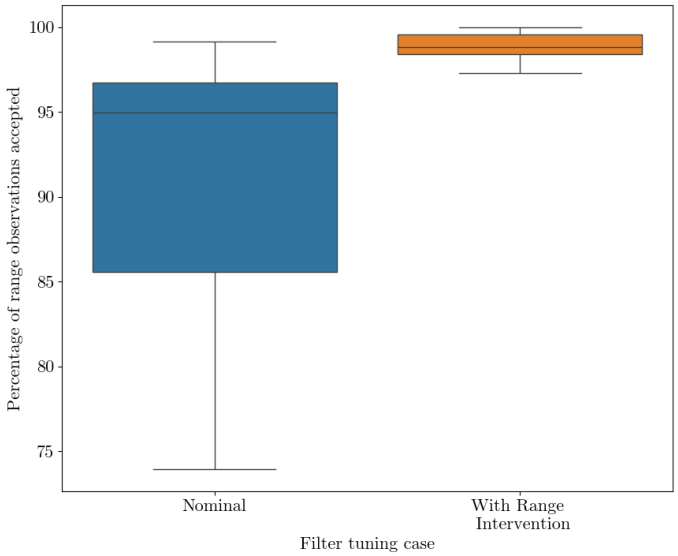

Figure 14: Percentage of range observations accepted without and with range rejection intervention.

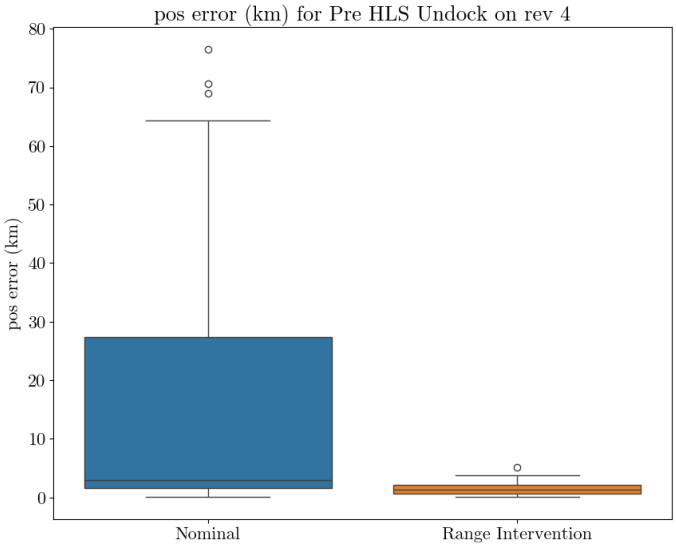

Figure 15: Position error at HLS undock for lunar sortie without and with range rejection intervention.

developed that rotates to be aligned with the spacecraft's Velocity-Normal-Binormal (VNB) frame. The velocity process noise magnitudes are defined with three values as the principal axes of an ellipsoid in the VNB frame. A rotation at every propagation step rotates the VNB-defined process noise values to inertial space (MJ2000) for integration into the covariance propagation. The result is a process noise that can be larger in certain rotating directions, and smaller for other rotating directions.

It has been shown that the positional covariance ellipsoid for a spacecraft within the NRHO has its principal axes roughly aligned with the VNB frame. The longest axis is in the velocity direction, and the shortest axis is in the normal direction.[11] The normal direction in the NRHO is also roughly the same direction as range observations. Recall earlier that the navigation filter can suffer from "filter collapse" in the range direction due to precise (low noise) but inaccurate (range biased) range observations in this orbital regime. The state estimate error in the range direction is thus not well-characterized by the filter covariance, with errors being consistently larger than the covariance expects.

It stands to reason that one way to prevent filter collapse could be to emphasize velocity process noise in the range direction. The process noise is identified as the principal axes of an ellipsoid aligned with the VNB frame and institute a larger magnitude for the rotating normal direction to increase uncertainty in roughly the range direction. To explore the impact of this process noise application, some scenarios that employ rotating process noise are executed in a monte carlo analysis to compare the data processing and error performance against the nominal spherical velocity process noise.

Several scenarios are explored that either adjust the baseline velocity process noise value or apply different values of rotating process noise. For this analysis, a more well-behaved scenario is explored with different process noise values to attempt to refine the navigation solution for higher accuracy (as opposed to building robustness against a stressing scenario). For the more well-behaved scenario, the logic is that lower velocity process noise values in the Velocity and Binormal directions

could limit unnecessary uncertainty growth and thus improve accuracy in those directions.

Figures 16 and 17 show the range observation acceptance statistics and position error at HLS undock on revolution 5 for four different process noise application regimes, respectively, on a scenario of the 2nd HLS mission timeline with a 1 mm/s body-fixed RCS perturbation model. The nominal scenario applies the same process noise to the timeline for the 1 mm/s body-fixed perturbation model results shown in Figure 13b. The High scenario doubles the nominal process noise values, applied spherically to the inertially defined state and covariance. The "VNB Low" and "VNB High" scenarios apply a rotating process noise aligned with the VNB frame. The "VNB Low" scenario reduces the Velocity and Binormal velocity process noise values and maintains the Normal direction process noise as equal to the Nominal scenario. This strategy is meant to reduce the overall process noise into the system and possibly refine the solution covariance. The "VNB High" scenario instead places the nominal process noise value in the Velocity and Binormal directions, and the doubled nominal value in the Normal direction.

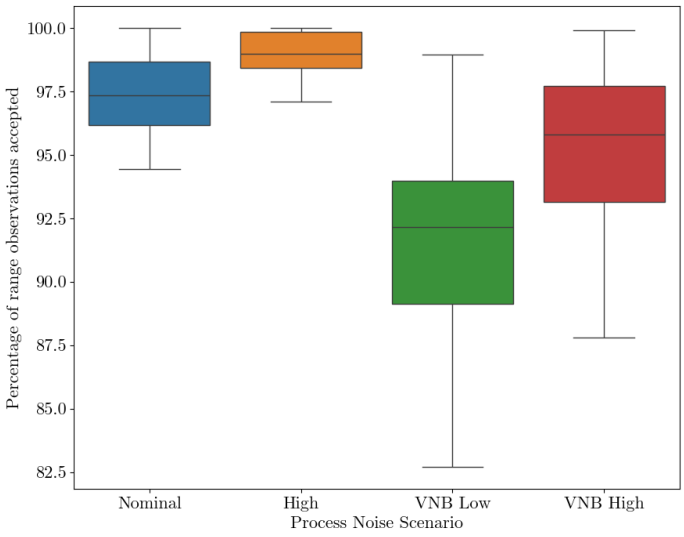

Figure 16: Percentage of range observations accepted under different process noise regimes.

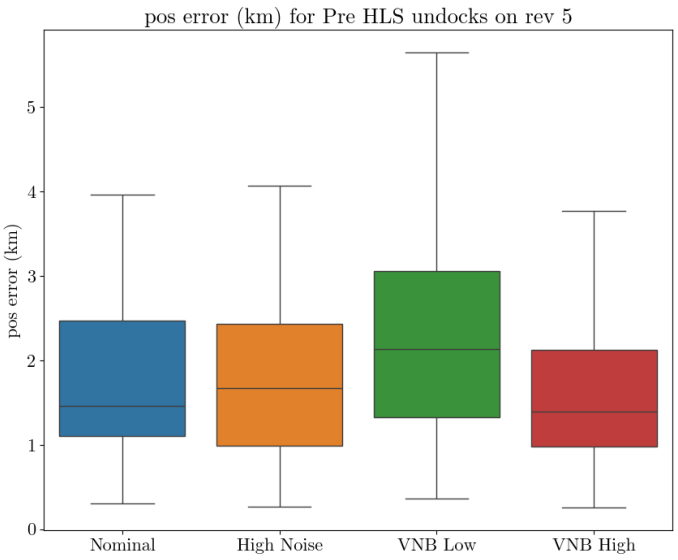

Figure 17: Position error at HLS undock for lunar sortie under different process noise regimes.

The introduction of rotating process noise does not significantly change the operational performance in this scenario. The "High" process noise scenario accepts more range observation data than the nominal scenario, suggesting that performance here is not negatively impacted by higher velocity process noise, and in fact higher process noise could still further improve performance. Despite the higher range observation acceptance rate, the error performance for the Pre HLS Undock event in Revolution 5 (shown in Figure 17) does not significantly change.

The "VNB Low" scenario performs the worst of the set, further suggesting that the issue for the supposed well-behaved scenario is not *too much* process noise. The range data performance and position error performance are noticeably worse. Finally, the "VNB High" scenario has an interesting result in that the data performance is worse than the nominal case, but the position error performance is essentially the same, with a slightly lower upper whisker.

CONCLUSION AND FORWARD WORK

Analyses of navigation performance of the Gateway under notional perturbation models are executed on simulations of two notional HLS mission timelines. A sensitivity analysis detailing the impact of error sources on the performance of the navigation system is executed for the two notional HLS mission timelines. Error sources are activated in sequence to isolate their impact to the total performance. These error sources include RPOD perturbations, CO_2 venting, notional RCS perturbations, and structural data blockage. It is found that HLS mission timeline A is more sensitive to the activation of error sources. This is partially due to the periods of time where the HLS is docked with Gateway without Orion, during which there is not constant tracking but there are many RCS perturbations pushing the true Gateway state away from the estimated state. Another problem for the first notional HLS mission timeline at its starting epoch is untimely structural blockage that causes a sharp rise in errors before the departure of HLS for the lunar sortie. The HLS mission timeline B is more robust against the inclusion of error sources. HLS arrives after Orion in this timeline, and its presence is nearly always constantly tracked while docked with Gateway. There is structural data blockage present in the second mission timeline, but the filter is more converged when encountering a structural data blockage, and more easily recovers afterward.

For each notional HLS mission timeline and for each notional RCS perturbation model (fully random or body fixed), monte carlo simulations are executed for incrementally increasing RCS perturbation magnitudes. The navigation filter was not re-tuned for each scenario of increasing RCS perturbation magnitude to more directly compare navigation filter performance changes. The navigation performance of the first mission timeline degrades as the random or body fixed RCS perturbation magnitude increased, as measured by the 3-σ editing acceptance rate of range observations, as shown in Figures 9a and 9b. The navigation performance for the second mission timeline is insensitive to RCS perturbation magnitude below RCS perturbation magnitudes of 10 mm/s and 2 mm/s for the random and body fixed models, respectively. This behavior is shown in Figures 13a and 13b.

Some additional navigation filter tuning methods are explored to improve performance. Range Rejection Intervention is a method that inflates the position covariance along the smallest principle axis whenever a range observation is 3-σ edited. This method is shown to improve navigation performance for the first mission timeline, as shown in Figures 14 and 15. Non-spherical and rotating application of velocity process noise to the navigation filter is employed, so that the process noise is defined in the VNB frame to adjust the Normal process noise relative to the Velocity and Binormal process noise values. This method does not significantly improve navigation performance, as shown in Figures 16 and 17.

These results are dependent on the notional mission timelines simulated, the assumptions of the RCS perturbation modeling, and the starting epoch of each mission. Forward work will focus on one mission timeline and explore the impact of mission starting epoch changes to navigation performance. The perturbation model will be refined and further explored through challenging the currently made assumptions in the model and timing. Finally, the sensitivity of the navigation performance to less tracking data, or loss of tracking data at different times of the mission will be explored. This and future work can help inform decisions for Gateway mission design as it relates to navigation requirements.

REFERENCES

[1] W. H. Gerstenmaier, "Progress in Defining the Deep Space Gateway and Transport Plan," https://www.nasa.gov/sites/default/files/atoms/files/nss_chart_v23.pdf, Mar. 28, 2017.

[2] R. Whitley and R. Martinez, "Options for Staging Orbits in Cis-Lunar Space," *2016 IEEE Aerospace Conference*, 2016.

[3] D. C. Davis, S. A. Bhatt, K. C. Howell, J. Jang, R. L. Whitley, F. D. Clark, D. Guzzetti, E. M. Zimovan, and G. H. Barton, "Orbit Maintenance and Navigation of Human Spacecraft at Cislunar Near Rectilinear Halo Orbits," *27th AAS/AIAA Space Flight Mechanics Meeting*, San Antonio, Texas, February 2017.

[4] N. Parrish, M. J. Bollinger, E. W. Kayser, M. R. Thompson, J. S. Parker, B. W. Cheetham, D. C. Davis, and D. J. Sweeney, "Near Rectilinear Halo Orbit Determination with Simulated DSN Observations.," *AIAA Scitech 2020 Forum*, Orlando, Florida, March 2020.

[5] M. J. Bollinger, M. R. Thompson, N. P. Ré, C. Ott, and D. C. Davis, "Ground-Based Navigation Trades for Operations in Gateway's Near Rectilinear Halo Orbit," *AAS/AIAA Astrodynamics Specialist Conference*, Big Sky, Virtual, August 2021.

[6] C. P. Newman, R. Sieling, D. C. Davis, and R. J. Whitley, "Attitude Control and Orbit Determination of a Crewed Spacecraft with Lunar Lander in Near Rectilinear Halo Orbit," *29th AAS/AIAA Space Flight Mechanics Meeting*, Ka'anapali, Hawaii, February 2019.

[7] D. C. Davis, F. S. Khoury, and K. C. Howell, "Phase Control and Eclipse Avoidance in Near Rectilinear Halo Orbits," *AAS Guidance, Navigation, and Control Conference*, Breckenridge, Colorado, February 2020.

[8] C. P. Newman, J. R. Hollister, F. S. Miguel, D. C. Davis, and D. J. Sweeney, "Attitude Control and Perturbation Analysis of a Crewed Spacecraft with a Lunar Lander in Near Rectilinear Halo Orbits," *AAS Guidance, Navigation, and Control Conference*, Breckenridge, Colorado, February 2020.

[9] J. Silva-Martinez, "Development of Space Mission Integrated Operations Scenarios," *17th International Conference on Space Operations*, Dubai, UAE, March 2023.

[10] C. P. Newman and D. C. Davis, "Attitude Control and Orbit Determination of a Crewed Spacecraft with Lunar Lander in Near Rectilinear Halo Orbit," *AAS Guidance, Navigation, and Control Conference*, Breckenridge, Colorado, February 2022.

[11] C. Ott, M. Bollinger, M. Thompson, and N. P. Re, "Range Biases, Measurement Noise, and Perilune Accuracy in Near Rectilinear Halo Orbit Navigation," *AIAA Scitech Forum and Exposition*, San Diego, California, January 2022.